Chinese Journal of Physiology 56(6): 341-348, 2013
DOI: 10.4077/CJP.2013.BAC194

Role of the Late Sodium Current in Rate-Dependent Repolarization of the Canine Ventricle

Hong Zhang[1], Lin Yang[2], Zhao Yang[3], and Xiao Zheng[1]

[1]*School of Electrical Engineering, Xi'an Jiaotong University, Xi'an 710049*
[2]*Cardiology Department, the First Hospital, Xi'an Jiaotong University, Xi'an 710061*
[3]*Institute of Medical Electronics in Medical School, Key Laboratory of Biomedical Information Engineering, Ministry of Education, Xi'an Jiaotong University, Xi'an 710061, Shaanxi People's Republic of China*

Abstract

Late sodium current I_{NaL} is an inward current participating in maintaining the plateau of the action potential. So far its role in the repolarization of canine hearts is not well known. In this paper, by taking advantage of a computer simulation method, we developed a one-dimensional transmural tissue to study the impacts of I_{NaL} on rate-dependent repolarization and its ionic basis in the canine ventricle. An OpenMP parallel algorithm was performed on a four-core personal computer to accelerate the simulation. The results demonstrated that action potential durations of midmyocytes showed greater rate dependence than the endo- and epi-myocytes. When the pacing rate was reduced, repolarization of the tissue was prolonged while the transmural dispersion of repolarization (TDR) was enlarged. The enhancement of I_{NaL} further amplified this rate-dependent repolarization and TDR meanwhile increased the risk of arrhythmogenesis. I_{NaL} was found highly sensitive to the pacing rate by calculating its kinetics. The study suggested that I_{NaL} played an important role in the rate-dependent repolarization of the canine ventricle. Selective blockade of I_{NaL} could have clinical benefits, especially for such pathological conditions with enhanced I_{NaL} as long QT 3 syndrome and heart failure.

Key Words: action potential, computer simulation, late sodium current, rate adaption, transmural heterogeneity

Introduction

Sudden cardiac death commonly occurs during the ventricular fibrillation characterized by multiple wavelets. But in the setting of a long QT (LQT) syndrome, a polymorphic ventricular tachycardia which is known as Torsade de Pointes (TdP) is also very lethal. LQT syndrome is a repolarization disorder with obvious prolongation of QT interval. It is observed not only in some pathological cardiac conditions, such as heart failure and ventricular hypertrophy, but also in Class III antiarrhythmic agents known as the drug-induced LQT (9).

It has long been recognized that some outward currents, such as the rapidly and slowly activating, delayed rectifier potassium currents I_{Kr} and I_{Ks} are the major currents responsible for ventricular muscle action potential repolarization (21). However, more and more evidences suggest the important role of an inward current, late sodium current I_{NaL} in the repolarization of rabbit hearts. I_{NaL} has been identified in ventricular cardiomyocytes of a large variety of mammalian species, including humans, dogs, rabbits, and rats. Although it is very small compared with the fast sodium component, its inactivation is very slow, usually lasting throughout the action potential, therefore, it also participates in repolarization of the action potential.

Corresponding author: Hong Zhang, Ph.D., School of Electrical Engineering, Xi'an Jiaotong University, 28 West Xianning Rd., Xi'an 710049, Shaanxi, People's Republic of China. E-mail: maxr@263.net
Received: January 9, 2013; Revised (Final Version): July 17, 2013; Accepted: August 8, 2013.
 ISSN : 0304-4920. http://www.cps.org.tw

Recently, Song *et al*. found that I_{NaL} significantly contributed to the action potential duration (APD) and pointed out that the effect of physiologic I_{NaL} on repolarization might be more important than currently appreciated (15). Undrovinas demonstrated that the inhibition of I_{NaL} by ranolazine could improve abnormal repolarization and contraction in canine failing heart (18). Moreover, I_{NaL} was found to increase in failing hearts and was implicated in the repolarization abnormalities (13, 17).

In other experiments (8, 22), by blocking I_{Kr} in rabbit hearts, they found that the repolarization exhibited the reverse rate-dependent (RRD) characteristics, that is, the repolarization prolongation became more distinct during bradycardia than during tachycardia. I_{NaL} rather than I_{Ks} was indicated to contribute to the RRD. In addition, the inhibition of I_{NaL} was found to markedly reduce the TdP liability in rabbit hearts.

Accordingly, I_{NaL} has recently received much concerns and resurged as a plausible target for cardioprotection (3, 14, 23). Despite its great fundamental and clinical importance, the role of I_{NaL} in ventricular repolarization and its rate property, especially in canine hearts are not well known. In this paper, by using the computer simulation method, we quantitatively investigated the effects of enhanced I_{NaL} on the canine ventricular repolarization and its ionic mechanisms.

Materials and Methods

Transmural Tissue Model

A canine single cell model (4) was chosen for our simulations. The model not only describes the traditional ionic channel activities and internal Ca^{2+} dynamics, but also presents the heterogeneity across the canine transmural tissue to approximate experimentally reported properties of endocardial, midmyocardial (M) and epicardial cells. Several new ionic currents, specifically, the late Na^{+} current are introduced. Compared with epicardium, I_{NaL} density was found large in endocardium, especially in M cells (25). Therefore, the model scales I_{NaL} maximal conductance to 1.25 and 1.7 of the epicardial value in endocardial and M cells, respectively.

In this study, a one-dimensional transmural tissue strand was developed based on the three single cell types. A total of 150 cells were arranged along the fiber from the left-hand to the right-hand ends. Cells from 1th to 50th were characterized with endocardium, 51th to 99th cells were M myocytes while the others were epicardium. Each simulated cell was electrically coupled with its two immediate neighbors by gap junctions (6). The whole length of the fiber was 15.0 mm due to the spatial step of 0.1 mm. Propagation of electrical excitation was described by the non-linear cable equation with the impermeable boundary conditions in Eq. 1.

$$\frac{\partial V}{\partial t} = -f(V,u)C_m^{-1} + D\frac{\partial^2 V}{\partial^2 x}$$
$$\frac{\partial V}{\partial x}\Big|_{x=x_{\min},x_{\max}} = 0 \qquad (1)$$

where D is the diffusion coefficient, x is spatial coordinates, and u is a vector of the gating variables and ionic concentrations that determine the total membrane current $f(V,u)$. $x_{\min}$ and $x_{\max}$ denote the left- and right-hand ends of the strand.

D of 0.25 mm^2/ms was set homogeneous throughout the strand except for a five-fold reduction at the M-to-epicardium border zone (cells 98th to 102th) (4).

Numerical Integration and Parallel Algorithm

To advance the integration efficiency, we used the operator splitting method to solve the equation. Euler method was applied to solve the membrane potential of each single cell while the three-point centered difference method was employed to integrate the partial differential equation describing the diffusion of action potentials (24). In the calculation, an adaptive time step method was used: if dV/dt >1 mV/ms, or within 5 ms after a stimulus current was applied, the time step Δt = 0.005 ms; within the time interval of 5 ms and 20 ms, Δt = 0.008 ms; during the other time interval Δt = 0.01ms.

In order to further improve the numerical accuracy, the second-order accuracy in space was used to discretize the boundary condition. The OpenMP parallel algorithm was performed on a four-core personal computer with Inter(R) Core(TM)2 Quad CPU Q8300 at a frequency of 2.5 GHz. C language and a set of compiler directives were used to program codes (21).

Extracellular Potentials

Extracellular unipolar potentials generated by the fiber in a conductive medium were computed from the transmembrane potential V using the following integral expression (6):

$$\phi = \frac{a^2}{4}\int(-\nabla V)\cdot[\nabla\frac{1}{x-x'}]dx \qquad (2)$$

where ϕ represents the unipolar potential recorded at an electrode 2 cm from the epicardial end of the strand, a is the radium of the fiber and x-x' is the

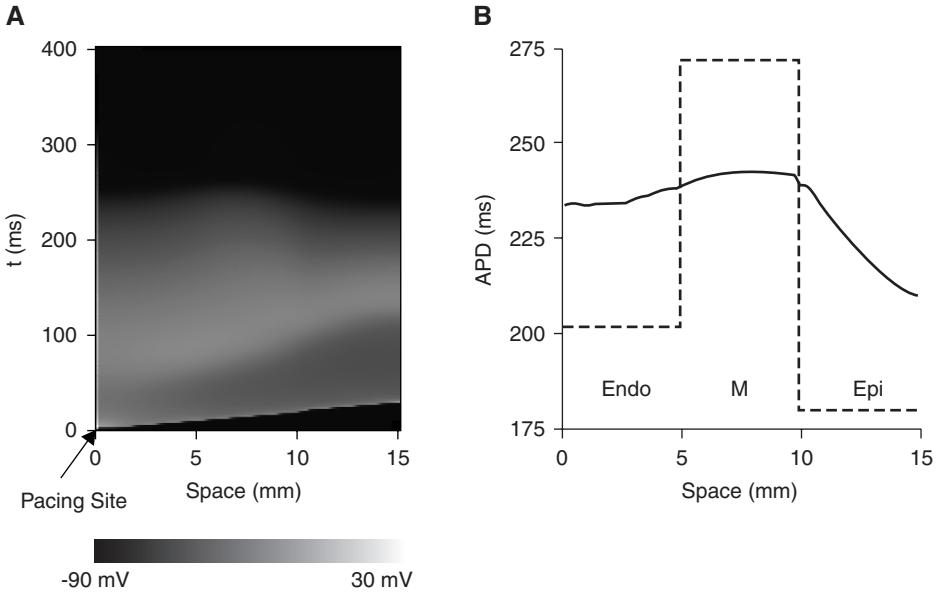

Fig. 1. Electrical activities along the developed heterogeneous transmural strand at the coupling interval of 1000 ms. A: computed space-time plot of response to the last pacing S1. B: transmural changes in APD along the coupled (solid line) and uncoupled (dashed line) strand.

distance from the electrode to any point in the fiber. The potential ϕ can constitute the ECG waveforms. To minimize stimulus and end effects, only cells 16th to 134th were included in our ECG computations.

Results

Electrical Behaviors across the Developed Tissue

Fig. 1 displays the excitation propagation (A) and action potential duration (B) across the transmural fiber with gap junctions coupled (solid line) and uncoupled (dashed line). The excitation was produced at the endocardial end by consecutive basic stimuli S1 with the basic cycle length (BCL) of 1000 ms. As noticed in Fig. 1A, S1 induced an electrical propagation from endocardium to epicardium, causing a propagation time delay upon the upstroke of action potentials at different sites. Three different type myocytes presented different action potential durations (APDs) in Fig. 1B. Endo-, mid- and epi-myocytes located in the middle of each layer had APDs of 235 ms, 243 ms and 221 ms, respectively, demonstrating a longest APD in mid-myocytes. However, due to homogenizing effects of cell-to-cell electrotonic coupling presented in the tissue, the smooth transitions in APD and repolarization between different layers could be observed in Fig. 1B except at the midmyocardial-epicardial border with a sudden reduced diffusion coefficient. Relative to the uncoupled single cells, APD dispersion was markedly reduced with cellular coupling.

Rate-Dependence of the Repolarization

Fig. 2 displays action potentials of three type myocytes and their corresponding ECG waveforms at pacing rates of 500 ms, 1000 ms and 2000 ms when I_{NaL} is in the control (A) and enhanced (B) conditions. As denoted, QT was defined as the time from the onset of the QRS to the end point of the T wave. $T_{p\text{-}e}$ was defined as the time from the peak to the end of the T wave. We noticed that in each situation, since the M cell had the longest APD, it repolarized last. Therefore, the onset and the end of the QT aligned with the upstroke of the endocardial action potential and the end point of the midmyocardial repolarization, respectively. In the meantime, complete repolarization of the epicardium and midmyocardium coincided with the peak and end of the T wave because of the earliest repolarization of the epicardium.

As noticed, APDs in either A or B showed a rate-dependent characteristic, especially for M cells. Compared with the results at BCL of 500 ms, APDs of the M cell at BCL = 1000 ms and 2000 ms increased 6.5% and 9.6% in the control condition (panel A), and 7.6% and 11.3% in the enhanced I_{NaL} situation (panel B), respectively. Meanwhile, QT and $T_{p\text{-}e}$ intervals prolonged with different extent when the pacing rate was reduced.

Additionally, with the rate slowing down a typical spike and dome (notch) morphology appeared at phase-1 of the action potential repolarization. It was most distinct for the epicardial cell. A J wave (Osborn wave) coincided with the notch in the epicardial

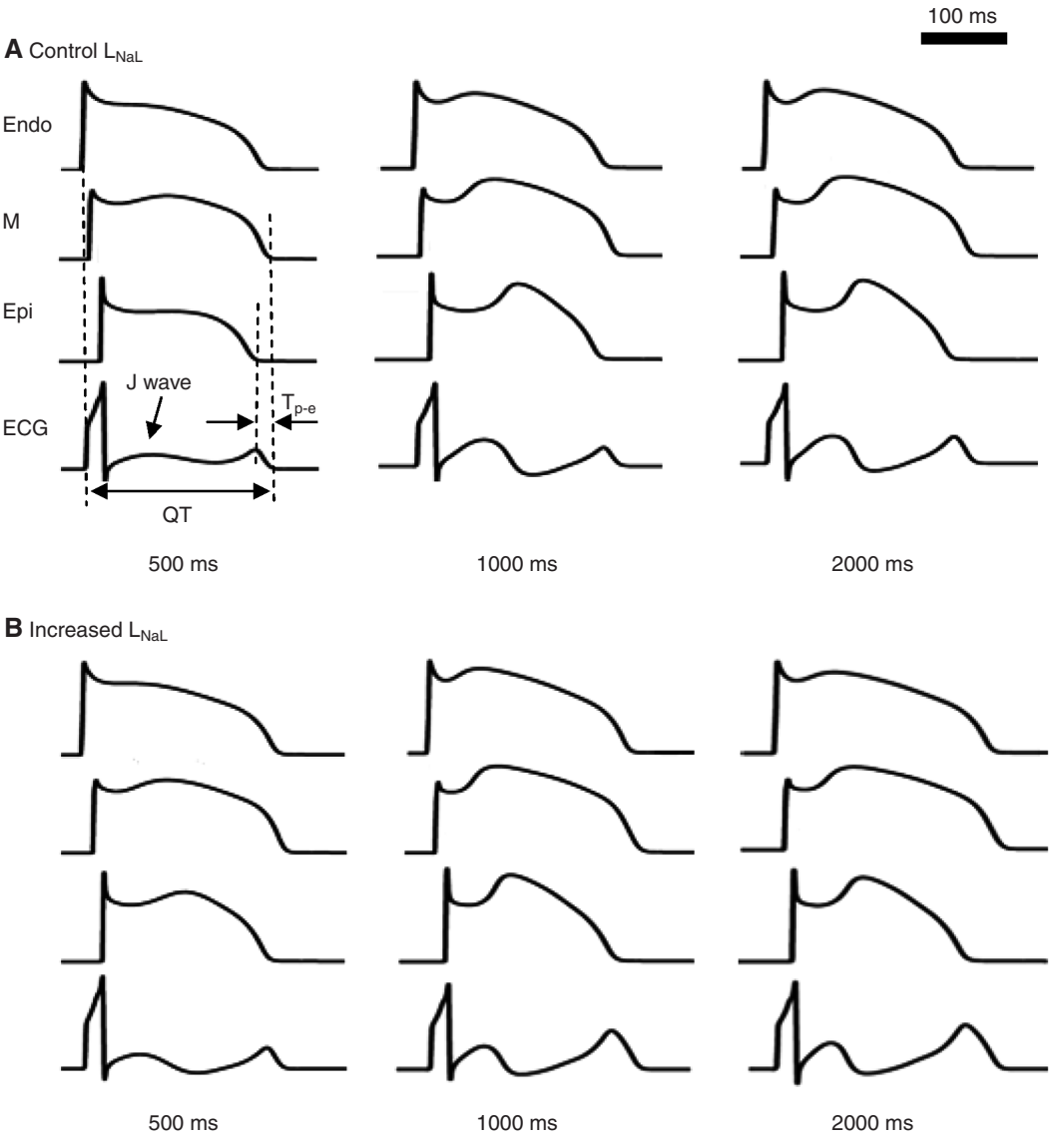

Fig. 2. Effects of I_{NaL} and pacing rates on action potential morphology and ECG waveforms. Panel A corresponds to the control condition. Panel B shows the results when I_{NaL} is doubled. In each panel, from the left to the right column the results at 3 different BCLs of 500 ms, 1000 ms, and 2000 ms are displayed. Action potentials of endocardial, M, and epicardial myocytes as well as the ECG are aligned from the top to the bottom in each column.

action potential was observed after each QRS complex in ECG. The notch and the J wave became more prominent at slow than at rapid rates, showing a bit of rate-dependence.

Effects of I_{NaL} on APDs, QT and T_{p-e} Intervals

In Fig. 2, in contrast to the panel A, when I_{NaL} was doubled (B), APDs lengthened, especially for M cells. Taking the BCL of 1000 ms as an example, compared with the corresponding APDs in A, APDs of the endo, M, and epi-myocardium in B increased about 4.5%, 6.6%, and 1.3%, respectively.

The relationship of QT and T_{p-e} intervals with BCLs at different I_{NaL} are presented in Fig. 3, A and B. The curves denoted with open triangles represent the control condition while the solid square and solid triangle labeled curves correspond to two and three times of I_{NaL}, respectively. As inspected, the more the I_{NaL} was enhanced, the more the QT was prolonged. Compared with the control I_{NaL}, for the doubled and tripled I_{NaL}, at BCL = 500 ms, QT increased about 5.1% and 9.6%, respectively; at BCL = 1000 ms, QT increased about 6.4% and 12.2%, respectively, while at BCL = 2000 ms, QT increased about 7.8% and 15.4%, respectively. So the increase in I_{NaL} and the increase in QT at a same BCL presented an approximately linear relationship. Besides, we observed that

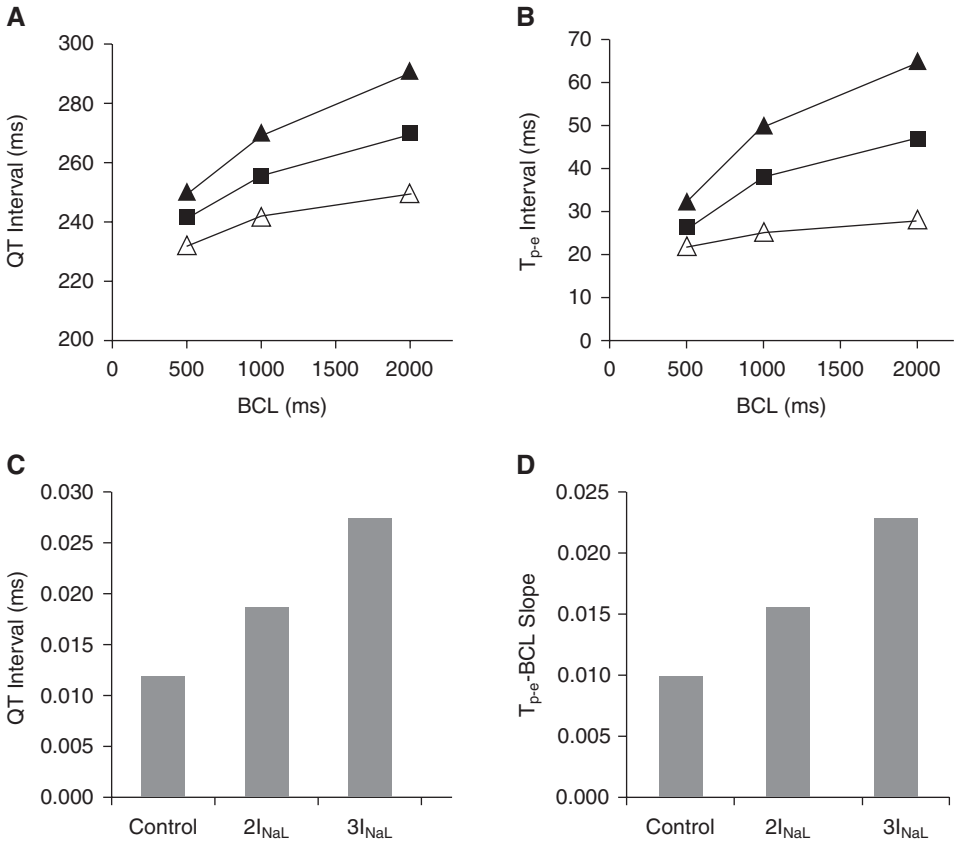

Fig. 3. Rate-dependent changes in QT (A) and T_{p-e} (B) when I_{NaL} is in the control (open triangle), doubled (solid square) and tripled (solid triangle) situations. C and D present the slopes of QT-BCL in A and T_{p-e}-BCL in B at the different I_{NaL}. The label of $2I_{NaL}$ represents the doubled I_{NaL} while $3I_{NaL}$ represents the tripled I_{NaL}.

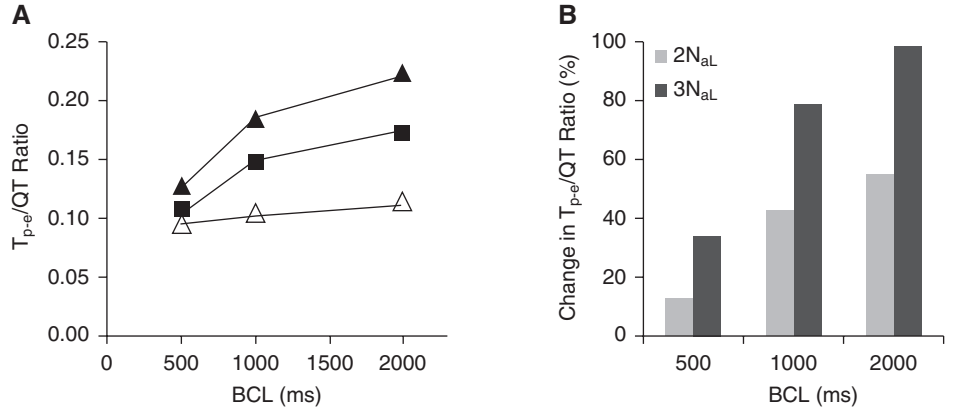

Fig. 4. T_{p-e}/QT ratio (A) and its change (B) with BCLs. In A, the open triangle labeled curve is the control condition while the solid square and solid triangle labeled curves represent the situations of doubled and tripled I_{NaL}, respectively.

at the same time, the prolongation became more significant at slow than at rapid rates. Slopes of QT-BCL and T_{p-e}-BCL shown in Fig. 3, C and D reflected that the change in QT and T_{p-e} as the function of BCLs became large with the increase of I_{NaL}.

Effects of I_{NaL} on T_{p-e}/QT Ratio

It was reported that the ratio of T_{p-e} to QT was an important arrhythmic index particularly relevant to the TdP risk of the LQT (7). Therefore, we calculated T_{p-e}/QT and its change ratio for the enhanced I_{NaL} in relative to the control condition. As presented in Fig. 4, larger I_{NaL} produced an obvious increase in T_{p-e}/QT and its change ratio. Compared with the

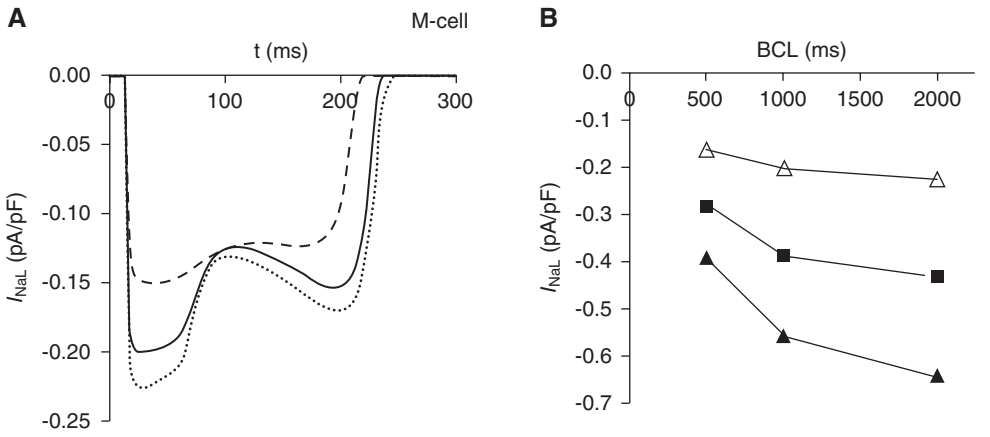

Fig. 5. Rate dependence of I_{NaL} in the M cell. I_{NaL} in the control condition is displayed in A: broken line for 500 ms, solid line for 1000 ms and dotted line for 2000 ms. B shows the relationship between the maximum I_{NaL} and the BCL in 3 different situations. The open triangle, solid square and solid triangle labeled curves represent situations of control, doubled and tripled I_{NaL}, respectively.

control condition, at BCL = 2000 ms, T_{p-e}/QT increased 54.9% and 103.6% in situations of doubled and tripled I_{NaL}, respectively. Besides, T_{p-e}/QT and its change ratio also presented a rate-dependent characteristic. In other words, they increased more with the rate slowing down.

I_{NaL} and Its Rate Dependence

In order to reveal the ionic basis that I_{NaL} contributed to the QT and T_{p-e} lengthening, particularly at the slow rate, we calculated the I_{NaL} current of the M cell at different BCLs since M cell is important in determining the tissue repolarization and has intrinsically largest I_{NaL}. Fig. 5A displays I_{NaL} at 3 different pacing rates in the control condition: 500 ms (broken line), 1000 ms (solid line) and 2000 ms (dotted line). Fig. 5B presents relationship of the maximum I_{NaL} current and the BCL in three cases: control (open triangle), two (solid square) and three (solid triangle) times of I_{NaL}, respectively. As noticed, I_{NaL} showed distinct rate dependence. The maximum I_{NaL} currents were about -0.16pA/pF, -0.20pA/pF and -0.22pA/pF at BCL of 500 ms, 1000 ms and 2000 ms, respectively. Therefore, under the control condition, the value of the maximum current increased about 38% from BCL of 500 ms to 2000 ms. The rate dependence became more significant when I_{NaL} was enhanced. In the situations of doubled and tripled I_{NaL}, the maximum current increased about 54% and 65% when BCL changed from 500 ms to 2000 ms, respectively.

Discussion

LQT syndrome is characterized by QT interval prolongation and susceptibility to sudden cardiac death due to TdP. Recently, the late sodium current I_{NaL} is postulated to generate prolonged action potentials and increased QT interval (12). In this paper, we developed a one-dimensional transmural canine tissue to quantitatively study the role of I_{NaL} in rate-dependent repolarization of the canine ventricle. In our model, three type myocytes exhibited different action potential morphology and durations. M cells presented the longest APD while epicardial cells showed the shortest one although their differences remarkably reduced due to electrotonic effects in the tissue (Fig. 1). Epicardium repolarized earlier than endocardium although the excitation sequence was inverse, thus, resulting in a positive T wave on ECG in our model. Besides, epicardium exhibited significant spike and dome morphology due to the large transient outward potassium current I_{to} (16).

It is known that repolarization of the mammalian ventricular cell often displays the physiological rate adaptive property, that is, tachycardia makes the APD and repolarization short while bradycardia makes them long. This phenomenon is also presented in our control conditions shown in Fig. 2A in which APD and repolarization represented by the QT interval on ECG both prolonged with the decrease of pacing rates. Furthermore, our results indicated that the transmural dispersion of repolarization (TDR) represented by T_{p-e} interval on ECG (1, 5) exhibited the rate adaptation at the same time. This property might be attributed to the M cell which showed more prominent rate-dependence than the other two cell types. In other words, at slower pacing rate, more time was required for the M cell to repolarize, thus lengthening the T_{p-e} interval which was determined by the repolarizing time differences between M and

epicardial cells.

In addition, in Fig. 2 the spike and dome morphology and the J wave on ECG became more obvious at BCL = 1000 ms than at BCL = 500 ms, suggesting a rate adaption of I_{to} since J wave was primarily formed by spike and dome which was determined by Ito. Thus, I_{to} was suggested to present a bit of rate-dependent property. However, if BCL was further increased, no obvious change in J wave was observed, indicating a limited contribution of I_{to} to the rate dependence.

Previously, it was popularly believed that I_{Ks} was a major modulator for the ventricular rate adaption (20). However, evidence suggested that in the canine ventricle, M cells showed much more rate dependent than the endo- and epi-myocardium although M cells have much smaller I_{Ks} than the other two cell types (10). In Fig. 2B, when I_{NaL} was doubled, APD, QT and T_{p-e} intervals lengthened and showed significant rate dependence compared with the results in Fig. 2A. Similarly, Fig. 3 demonstrated that with further increase of I_{NaL}, repolarization prolongation and dispersion of repolarizing both were amplified much more during bradycardia than during tachycardia. These all suggested that I_{NaL} played an important role in modulation of the rate-dependence in the canine heart, particularly for the M cell that presents intrinsically large I_{NaL} and small I_{Ks}.

TDR and RRD have been observed in studies (1, 19). Previous findings found that the inhibition of the sodium current could reduce TDR (11). Together with the experiment in rabbit hearts (8) and our simulations in canine hearts, we suggested that TDR and RRD at least partially attributed to the heterogeneous distribution of I_{NaL} along the transmural wall. Since the different I_{NaL} density among three type myocytes, the response to the pacing rate was different, resulting in a rate-dependent TDR. It is well known that TDR plays an important role in forming reentrant arrhythmia, therefore, the increase in TDR at the slow rate might raise the possibility of the occurrence of TdP. Our simulations revealed that the risk of occurring TdP increased during bradycardia than during tachycardia, and with the enhancement of I_{NaL} the risk could be elevated (Fig. 4). This might attribute to the enlarged TDR which was caused by enhanced I_{NaL} at slow rate. In other reports, I_{NaL} was supposed to contribute to triggering arrhythmia in two ways (17). One was by causing early afterdepolarisations (EAD) due to the repolarizing prolongation. The other way might be causing late afterdepolarisations (DAD) attributable to calcium oscillations in sodium-calcium overload conditions. Therefore, either for the reentrant or triggered arrhythmia, inhibition of I_{NaL} would be suggested to have possibility to low the arrhythmogenesis, thereby potentially having clinical benefits, especially for the LQT3 (enhanced I_{NaL}) (2) and other pathological conditions with enhanced I_{NaL}, such as heart failure.

As an important inward current in maintaining the plateau of the action potential, I_{NaL} has so far received little attention in modulation of rate dependence. Our simulation investigated the kinetics of I_{NaL} and its changes in maximum amplitude with BCLs. As displayed in Fig. 5, I_{NaL} was highly dependent on BCLs. This dependence was amplified by the enhancement of I_{NaL}. This from the ionic basis revealed that I_{NaL} was indeed sensitive to the pacing rate.

In our simulation, we didn't investigate the role of I_{Kr} and I_{Ks} in the rate-dependent repolarization. I_{Kr} and I_{Ks} were kept same for different I_{NaL} at different pacing rates. Therefore, for a same pacing rate, their contributions to repolarization were approximately the same in the situations of control, doubled or tripled I_{NaL}. Besides, compared with Epi and Endo cells, M cells have small I_{Ks} but large I_{NaL}. Now M cells were found to show more distinct rate dependence than the other 2 cell types. So we could tell that the contribution of I_{NaL} to rate-dependent repolarization was great, especially in situations of enhanced I_{NaL}. Therefore, our results are not expected to be influenced by the function of I_{Kr} and I_{Ks} in the repolarization. However, I_{Kr} and I_{Ks} are outward currents that also participate in repolarization of the action potential. They have different densities across the transmural wall which might contribute to the heterogeneity of repolarization. So their roles in the rate-dependent repolarization and TDR are also important and would be expected in our future work.

In summary, our simulation demonstrated that I_{NaL} itself showed rate dependent property. It played an important role in the rate-dependent repolarization of canine hearts. The enhancement of I_{NaL} could amplify the risk of arrhythmogenesis. Accordingly, selective blockade of I_{NaL} was indicated to be a potential target for antiarrhythmic therapy.

Acknowledgments

This study was supported by the National Natural Science Foundation of China (Nos. 81271661, 30870659, 30971221), the Health Foundation of Shaanxi province in China (08D23), the Scientific Research Foundation for the Returned Overseas Chinese Scholars, State Education Ministry (SRF for ROCS, SEM), and the Fundamental Research Funds for the Central Universities.

References

1. Antzelevitch, C., Sicouri, S., Di Diego, J.M., Burashnikov, A.,

Viskin, S., Shimizu, W., Yan, G.X., Kowey, P. and Zhang, L. Does Tpeak-Tend provide an index of transmural dispersion of repolarization? *Heart Rhythm* 4: 1114-1116, 2007.

2. Bankston, J.R., Sampson, K.J., Kateriya, S., Glaaser, I.W., Malito, D.L., Chung, W.K. and Kass, R.S. A novel LQT-3 mutation disrupts an inactivation gate complex with distinct rate-dependent phenotypic consequences. *Channels (Austin)* 1: 273-280, 2007.
3. Belardinelli, L., Shryock, J.C. and Fraser, H. Inhibition of the late sodium current as a potential cardioprotective principle: effects of the late sodium current inhibitor ranolazine. *Heart* 92: iv6-iv14, 2006.
4. Benson, A.P., Aslanidi, O.V., Zhang, H. and Holden, A.V. The canine virtual ventricular wall: a platform for dissecting pharmacological effects on propagation and arrhythmogenesis. *Prog. Biophys. Mol. Biol.* 96: 187-208, 2008.
5. Chen, X.Z., Zhang, H., Jin, Y.B. and Yang, L. Vulnerability to unidirectional conduction block and reentry in rabbit left ventricular wedge preparation: effects of stimulation sequence and location. *Chinese J. Physiol.* 52: 16-22, 2009.
6. Gima, K. and Rudy, Y. Ionic current basis of electrocardiographic waveforms: a model study. *Circ. Res.* 90: 889-896, 2002.
7. Gupta, P., Patel, C., Patel, H., Narayanaswamy, S., Malhotra, B., Green, J.T. and Yan, G.X. T(p-e)/QT ratio as an index of arrhythmogenesis. *J. Electrocardiol.* 41: 567-574, 2008.
8. Jia, S., Lian, J., Guo, D., Xue, X., Patel, C., Yang, L., Yuan, Z., Ma, A. and Yan, G.X. Modulation of the late sodium current by ATX-II and ranolazine affects the reverse use-dependence and proarrhythmic liability of I_{Kr} blockade. *Brit. J. Pharmacol.* 164: 308-316, 2011.
9. Kannankeril, P., Roden, D.M. and Darbar, D. Drug-induced long QT syndrome. *Pharmacol. Rev.* 62: 760-781, 2010.
10. Liu, D.W. and Antzelevitch, C. Characteristics of the delayed rectifier current (I_{Kr} and I_{Ks}) in canine ventricular epicardial, midmyocardial, and endocardial myocytes. A weaker I_{Ks} contributes to the longer action potential of the M cell. *Circ. Res.* 76: 351-365, 1995.
11. Liu, T., Brown, B.S., Wu, Y., Antzelevitch, C., Kowey, P.R. and Yan, G.X. Blinded validation of the isolated arterially perfused rabbit ventricular wedge in preclinical assessment of drug-induced proarrhythmias. *Heart Rhythm* 3: 948-956, 2006.
12. Lowe, J.S., Stroud, D.M., Yang, T., Hall, L., Atack, T.C. and Roden, D.M. Increased late sodium current contributes to long QT-related arrhythmia susceptibility in female mice. *Cardiovasc. Res.* 95: 300-307, 2012.
13. Maltsev, V.A. and Undrovinas, A. Late sodium current in failing heart: friend or foe? *Prog. Biophys. Mol. Biol.* 96: 421-451, 2008.
14. Moreno, J.D. and Clancy, C.E. Pathophysiology of the cardiac late Na current and its potential as a drug target. *J. Mol. Cell. Cardiol.* 52: 608-619, 2012.
15. Song, Y., Shryock, J.C. and Belardinelli, L. Late sodium current is an intrinsic regulator of cardiac repolarization—a quantitative assessment. *Heart Rhythm* 9: 1909-1921, 2012.
16. Sun, X. and Wang, H.S. Role of the transient outward current (Ito) in shaping canine ventricular action potential—a dynamic clamp study. *J. Physiol.* 564: 411-419, 2005.
17. Undrovinas, A. and Maltsev, V.A. Late sodium current is a new therapeutic target to improve contractility and rhythm in failing heart. *Cardiovasc. Hematol. Agents Med. Chem.* 6: 348-359, 2008.
18. Undrovinas, A.I., Belardinelli, L., Undrovinas, N.A. and Sabbah, H.N. Ranolazine improves abnormal repolarization and contraction in left ventricular myocytes of dogs with heart failure by inhibiting late sodium current. *J. Cardiovasc. Electrophysiol.* 17: S169-S177, 2006.
19. Virag, L., Acsai, K., Hala, O., Zaza, A., Bitay, M., Bogats, G., Papp, J.G. and Varro, A. Self-augmentation of the lengthening of repolarization is related to the shape of the cardiac action potential: implications for reverse rate dependency. *Brit. J. Pharmacol.* 156: 1076-1084, 2009.
20. Viswanathan, P.C., Shaw, R.M. and Rudy, Y. Effects of I_{Kr} and I_{Ks} heterogeneity on action potential duration and its rate dependence: a simulation study. *Circulation* 99: 2466-2474, 1999.
21. Wang, J., Zhang, H., Wu, R.J., Yang, L. and Liu, Y.B. Study of parallel algorithm based on openMP in myocardial simulation. *Adv. Mater. Res.* 204: 1584-1587, 2011.
22. Wu, L., Ma, J., Li, H., Wang, C., Grandi, E. and Zhang, P. Late sodium current contributes to the reverse rate-dependent effects of Ikr inhibition on ventricular repolarization. *Circulation* 123: 1713-1720, 2011.
23. Xi, Y., Wu, G., Yang, L., Han, K., Du, Y., Wang, T., Lei, X., Bai, X. and Ma, A.Q. Increased late sodium currents are related to transcription of neuronal isoforms in a pressure-overload model. *Eur. J. Heart Fail.* 11: 749-757, 2009.
24. Zhang, H., Wang, J., Yang, L., Wu, R.J., Mei, X. and Zhao, W. Vulnerability in simulated ischemic ventricular transmural tissues. *Chinese J. Physiol.* 54: 427-434, 2011.
25. Zygmunt, A.C., Eddlestone, G.T., Thomas, G.P., Nesterenko, V.V. and Antzelevitch, C. Larger late sodium conductance in M cells contributes to electrical heterogeneity in canine ventricle. *Am. J. Physiol. Heart Circ. Physiol.* 281: H689-H697, 2001.